고차 축대칭 경계 요소에 의한 소형 터보젯 엔진의 터빈 로우터 디스크 해석

Higher Order Axismmetric Boundary Element Analysis of Turbine Rotor Disk of the Small Turbojet Engine

Kim Jin-Woo
(Advanced Institute of Military Science and Technology)

요 약

일반적인 선형 탄성해석 경계 요소법이 초 고속 회전과 정상 열전도에 의한 열 탄성 효과가 고려된 문제에 적용되었다. 축대칭 경계 요소법 구성이 요약되었고, 등가 경계 적분 방정식의 물체력 핵 함수의 체적 적분 전환 방법에 일반화된 내적과 벡터 연산법 개념이 도입되었다. 고차 경계 요소 적용을 위한 이산화 수치 해석법이 요약되었고, 소형 젯트 엔진(ADD 500)의 터어빈 로우터 디스크의 해석 결과가 유한 요소해와 비교되었다.

Key Words : 고차 축대칭 경계 요소법, 열 탄성 핵함수, 회전 관성 핵함수, 소형 터보젯 엔진의 터어빈 로오타 디스크

ABSTRACT

The BEM for linear elastic stress analysis is applied to the highly rotating axisymmetric body problem which also involves the thermoelastic effects due to steady-state thermal conduction. The axisymmetric BEM formulation is briefly summarized and an alternative approach for transforming the volume integrals associated with such body force kernels into equivalent boundary integrals is described in a way of using the concept of inner product and vector identity. A discretization scheme for higher order BE is outlined for numerical treatment of the resulting boundary integral equations, and it is consequently illustrated by determining the stress distributions of the turbine rotor disk of the small turbojet engine(ADD 500) for which a FEM stress solution has been furnished by author.

Key Words : Higher Order Axisymmetric BEM, Thermoelastic Kernel, Rotational Inertia Kernel, Turbine Rotor Disk of the Small Turbojet Engine.

1. INTRODUCTION

In a class of stress analysis problems, axisymmetric elastic bodies are subjected to boundary tractions and displacements as well as thermal and centrifugal body forces. The strength design of gas turbojet engines involves a large number of axisymmetric parts such as the compressor and turbine disks. It is clear in stress analysis of such a turbine rotor disk that inclusion of rotational inertia body force loading and steady-state thermoelastic effects is of major importance.

Application of the Boundary Element Method(BEM) to thermoelastic and centrifugal axisymmetric loading problems was first formulated by Cruse et al.[1] but limited numerical implementation to linear elements sometimes circular arcs in shape. Further developments included the use of isoparametric quadratic elements for themoelastic problems(Bakr and Fenner[2]) and rotating axisymmetric body problems (Abdul-Mihsein et al.[3]). Numerical examples are however confined to simple axisymmetric geo- metries such as thick-walled cylinder, hollow sphere, and rotating disk of uniform thickness, and centrifugal body force and thermal loading problems are treated separately.

The main purpose of present study is to determine the stresses of the turbine rotor disk of turbojet engine subjected to both thermal and highly rotational inertia force by the axisymmetric BEM. While the formulation of the method follows closely in spirit the ideas outlined for thermoelastic analysis by Bakr and Fenner[2] and centrifugal loading by Abdul-Mihsein et al.[3], combination of two loadings is magnified by numerical procedure for higher order BE. The development of the axisymmetric BEM is summarize in order to motivate the subsequent numerical extension to thermoelastic rotating axisymmetric body problems and new procedure for deriving the fundamental thermal and centrifugal body force kernels on equivalent boundary integral is presented in a efficient way of using the concept of inner product and invariant vector operation. Finally axisymmetric BEM solutions to the model problem of the turbine rotor disk in small turbojet engine(ADD 500) are presented and compared with the axisymmetric FEM solutions.

2. AXISYMMETRIC BEM FORMULATIONS

Consider an axisymmetric body of arbitrary cross-sectional shape with an interior point p in Ω and a boundary point Q on $\partial\Omega$ as shown in Fig.1. Following the analysis of the weighted residual statements or the Betti's reciprocal theorem, the interior displacement solution formula can be obtained known as the Somigliana integral for centrifugal and thermoelastic loading(Cruse et al.[1]) which is

given by

$$u_i(p) = -\int_{\partial\Omega} T_{ji}(p,Q)\ u_j(Q)ds + \int_{\partial\Omega} U_{ji}(p,Q)\ t_j(Q)ds + \rho\,\omega^2 \int_{\Omega} U_{ji}(p,q)\ x_i(q)dV + \frac{\alpha E}{1-2\nu}\int_{\Omega} U_{ji,j}(p,q)\,\Phi(q)dV \quad (1)$$

where u_i is the displacements, t_i is the tractions, Φ is the temperature and x_i is the location relative to the center of rotation of q in Ω. The constants are mass density ρ, angular velocity ω, Poisson's ratio ν, Young's modulus E and coefficient of thermal expansion α, T_{ji} and U_{ji} are the traction and displacement kernel functions associated with the three dimensional fundamental solutions to the Navier's equation of equilibrium.

Fig. 1 Geometry of the axisymmetric solution domain

For the axisymmetric BEM formulation two alternative approaches have been used to derive the kernel functions. The first(Rizzo and Shippy[4]) is to integrate the three dimensional Kelvin's solutions along the circular path around the axis of rotational symmetry. The second approach is to obtain the axisymmetric component form of Galerkin vector directly(Kermanidis[5], Cruse et al.[1]) and is the one used here. As described in the second approach the complementary displacement vector $\underline{u}^*$ associated with the displacement kernel can be represented in terms of Galerkin vector $\underline{G}$ as

$$\underline{u}^* = \nabla^2 \underline{G} - \frac{1}{2(1-\nu)} \nabla(\nabla \cdot \underline{G}) \quad (2)$$

Then substitution of this expression into the Navier's equation gives the following biharmonic equations in radial $-r$ and axial $-z$ direction, respectively

$$\left(\nabla^2 - \frac{1}{r^2}\right)\left(\nabla^2 - \frac{1}{r^2}\right) G_r = -\frac{F_r}{\mu}$$

$$\nabla^2 \nabla^2 G_z = -\frac{F_z}{\mu} \quad (3)$$

where (G_r , G_z) are the Galerkin vector components, (F_r , F_z) are the fundamental body force components which can be represented through the use of Dirac delta function, and μ is shear modulus. Integral transform methods(ex. Hankel transform by Bakr and Fenner[2]) can be then used to obtain solutions for (G_r , G_z) from Eq.(3) and the results are given in terms of Legendre functions of the second kind

$$G_r = \sqrt{(Rr)}\sqrt{(r^2-1)}\,\frac{Q^{-1}_{+1/2}(Y)}{8\pi^2\mu}$$

$$G_z = \sqrt{(Rr)}\sqrt{(r^2-1)}\,\frac{Q^{-1}_{-1/2}(Y)}{8\pi^2\mu} \quad (4)$$

$$Y = 1 + \frac{[(Z-z)^2 + (R-r)^2]}{2Rr}$$

where (R, Z) represent the coordinate components of load point p and (r, z) represent the field point q in Ω. The displacement kernels U_{ij} are then determined by substitution of Eq.(4) into the relations

$$
\begin{aligned}
&2(1-\nu)\,U_{rr} \\
&\quad=(1-2\nu)\left(\nabla^2-\frac{1}{r^2}\right)G_r+\frac{\partial^2 G_r}{\partial z^2} \\
&2(1-\nu)\,U_{zr} \\
&\quad=-\frac{\partial^2 G_r}{\partial r\,\partial z}-\left(\frac{1}{r}\right)\frac{\partial G_r}{\partial z} \\
&2(1-\nu)\,U_{rz}=-\frac{\partial^2 G_z}{\partial r\,\partial z} \qquad (5)\\
&2(1-\nu)\,U_{zz}=(1-2\nu)\nabla^2 G_z \\
&\qquad+\frac{\partial^2 G_z}{\partial r^2}+\left(\frac{1}{r}\right)\frac{\partial G_z}{\partial r}
\end{aligned}
$$

Now the volume integrals of last two terms in Eq.(1) limits the potential benefits of BEM formulation. In order to reduce the volume integrals to equivalent boundary integrals in Eq.(1) it is convenient to use the concept of inner product of body force and fundamental displacement. The first volume integral in Eq.(1) associated with the body force vector for rotational inertia loading has the following inner product of body force $\underline{b}$ and fundamental displacement $\underline{u}^*$

$$
\begin{aligned}
<\underline{b},\underline{u}^*>_\Omega &= \rho\omega^2\int_\Omega(\underline{x}\cdot\underline{u}^*)\,dV \\
&=\rho\omega^2\int_\Omega\left[\nabla^2\underline{G}-\frac{1}{2(1-\nu)}\underline{\nabla}(\underline{\nabla}\cdot\underline{G})\right]\cdot\underline{x}\,dV \qquad (6)
\end{aligned}
$$

Substitution of the following vector identity

$$
\underline{\nabla}(\underline{\nabla}\cdot\underline{G}) = \nabla^2\underline{G}+\underline{\nabla}\times(\underline{\nabla}\times\underline{G}) \qquad (7)
$$

and Green theorem for volume integrals to surface integrals

$$
\begin{aligned}
&\int_\Omega \underline{x}\cdot[\,\underline{\nabla}\times(\underline{\nabla}\times\underline{G})]\,dV \\
&\quad=\int_{\partial\Omega}\underline{x}\cdot(\underline{n}\times\underline{\nabla}\times\underline{G})\,dS \\
&\int_\Omega \underline{x}\cdot\nabla^2\underline{G}\,dV \qquad (8)\\
&\quad=\int_{\partial\Omega}[\underline{x}(\underline{\nabla}\cdot\underline{G}-\underline{G}(\underline{\nabla}\cdot\underline{x}))]\cdot\underline{n}\,dS \\
&\qquad-\int_\Omega[\underline{x}\cdot\underline{\nabla}\times(\underline{\nabla}\times\underline{G})]\,dV
\end{aligned}
$$

Eq.(6) can be then directed to the equivalent boundary integral

$$
\begin{aligned}
&\rho\omega^2\int_\Omega\underline{x}\cdot\underline{u}^*\,dV = \\
&\quad\rho\omega^2\frac{(1-2\nu)}{2(1-\nu)}\int_{\partial\Omega}[\underline{x}(\underline{\nabla}\cdot\underline{G}-\underline{G}(\underline{\nabla}\cdot\underline{x}))]\cdot\underline{n}\,dS \\
&\qquad-\rho\omega^2\int_{\partial\Omega}\underline{x}\cdot(\underline{n}\times\underline{\nabla}\times\underline{G})\,dS \qquad (9)
\end{aligned}
$$

In order to reduce the second volume integral in Eq.(1) consider thermal body force and boundary traction of heat flux

$$
\underline{b}=-\frac{\alpha E}{(1-2\nu)}\underline{\nabla}\Phi,\quad \underline{t}=\frac{\alpha E}{(1-2\nu)}\Phi\,\underline{n} \qquad (10)
$$

Then application of two inner product of above thermoelastic effects and fundamental displacement $< \underline{b}, \underline{u}^* >_{\Omega}$, $< \underline{t}, \underline{u}^* >_{\partial\Omega}$ to the Betti's reciprocal theorem being the basis for derivation of Somigliana identity yields an equivalent representation to the second volume integral in terms of invarient vector form as

$$\frac{\alpha E}{(1-2\nu)} \int_{\Omega} \Phi(\nabla \cdot \underline{u}^*)\, dV = \frac{\alpha E}{(1-2\nu)} \int_{\Omega} \Phi\{\nabla \cdot [\nabla^2 \underline{G} - \frac{1}{2(1-\nu)} \nabla(\nabla \cdot \underline{G})]\}\, dV \tag{11}$$

Use of the vector identity such as $\underline{\nabla} \cdot (\nabla^2 \underline{G}) = \nabla^2(\underline{\nabla} \cdot \underline{G})$ and condition of steady-state heat conduction $\nabla^2 \Phi = 0$ in Ω. Proceeding the same argument to Green theorem, Eq.(11) can be finally reduced to the following boundary integral equation

$$\frac{\alpha E}{(1-2\nu)} \int_{\Omega} \Phi(\nabla \cdot \underline{u}^*)\, dV = \frac{\alpha E}{2(1-\nu)} \int_{\partial\Omega} [\Phi \nabla(\nabla \cdot \underline{G}) - (\nabla \cdot \underline{G}) \nabla \Phi] \cdot \underline{n}\, dS \tag{12}$$

These two transformed Eqs.(9) and (12) can be utilized to construct the corresponding boundary integral formula for the displacement.

Reduction of Somigliana identity of Eq.(1) to the boundary integral representation is accomplished by taking the limit of each term as the interior point p approaches a boundary point P. The resulting integral equations for the boundary displacement can be expressed as

$$C_{ij}(P)\, u_j(P) = \int_{\partial\Omega} [\, U_{ij}(P,Q)\, t_j(Q) - T_{ij}(P,Q)\, u_j(Q) + \alpha\, V_{ij}(P,Q)\, \Phi_j(Q) + \rho\, \omega^2\, W_i(P,Q)]\, dS \tag{13}$$

where the subscripts i and j range over r and z except temperature Φ_1, normal derivative of $\Phi_2 = \underline{\nabla} \Phi \cdot \underline{n}$. The thermal loading kernels V_{ij} and rotational inertia force kernels W_i are defined from Eqs.(12) and (9), respectively. The coefficients C_{ij} can be evaluated in the limiting process used in deriving boundary integral equation. This procedure is described in detail by Cruse et al.[1] and Hartmann[7].

3. NUMERICAL TREATMENT AND RESULTS

The boundary contour $\partial\Omega$ of the typical θ-plane in axisymmetric body is divided into elements and the integration of Eq.(13) performed over each element. The coordinates of any point on the element can be expressed in terms of the usual quadratic interpolation functions as

$$r(\xi) = N_i(\xi)\, r_i \; ; \quad z(\xi) = N_i(\xi)\, z_i$$

where

$$N_1(\xi)=\frac{1}{2}(1-\xi)-\frac{1}{2}(1-\xi^2)$$
$$N_2(\xi)=\frac{1}{2}(1+\xi)-\frac{1}{2}(1-\xi^2) \quad (14)$$
$$N_3(\xi) = (1-\xi^2)$$

Similarly the displacement and traction can be also represented as

$$u_r(\xi)=N_i(\xi)\,u_{ri}\;;\quad u_z(\xi)=N_i(\xi)\,u_{zi}$$
$$t_r(\xi)=N_i(\xi)\,t_{ri}\;;\quad t_z(\xi)=N_i(\xi)\,t_{zi} \quad (15)$$

The descretization of the boundary integral equation of (13) can consequently yields in axisymmetric form

where M is the total number of elements, and $J(\xi)$ is the Jacobian of transformation.

$$C_{rr}(P)\,u_r(P)+C_{rz}(P)\,u_z(P) =$$

$$2\pi\sum_{m=1}^{M}\sum_{n=1}^{3}\left[\begin{array}{l} -u_{r\,n}^{m}(Q)\int_{-1}^{+1}T_{rr}(P,Q(\xi)) \\ -u_{z\,n}^{m}(Q)\int_{-1}^{+1}T_{rz}(P,Q(\xi)) \\ +t_{r\,n}^{m}(Q)\int_{-1}^{+1}U_{rr}(P,Q(\xi)) \\ +t_{z\,n}^{m}(Q)\int_{-1}^{+1}U_{rz}(P,Q(\xi)) \\ +\Phi_{n}^{m}(Q)\int_{-1}^{+1}V_{r1}(P,Q(\xi)) \\ +\frac{d\Phi}{dn}{}_{n}^{m}(Q)\int_{-1}^{+1}V_{r2}(P,Q(\xi)) \\ +\rho\omega^2\frac{(1-2\nu)}{2(1-\nu)}\int_{-1}^{+1}W_1(P,Q(\xi)) \\ +\rho\omega^2\int_{-1}^{+1}W_2(P,Q(\xi)) \end{array}\right] N_m(\xi)r(\xi)J(\xi)d\xi \quad (16)$$

$$C_{zr}(P)\,u_r(P)+C_{zz}(P)\,u_z(P) =$$

$$2\pi\sum_{m=1}^{M}\sum_{n=1}^{3}\left[\begin{array}{l} -u_{r\,n}^{m}(Q)\int_{-1}^{+1}T_{zr}(P,Q(\xi)) \\ -u_{z\,n}^{m}(Q)\int_{-1}^{+1}T_{zz}(P,Q(\xi)) \\ +t_{r\,n}^{m}(Q)\int_{-1}^{+1}U_{zr}(P,Q(\xi)) \\ +t_{z\,n}^{m}(Q)\int_{-1}^{+1}U_{zz}(P,Q(\xi)) \\ +\Phi_{n}^{m}(Q)\int_{-1}^{+1}V_{z1}(P,Q(\xi)) \\ +\frac{d\Phi}{dn}{}_{n}^{m}(Q)\int_{-1}^{+1}V_{z2}(P,Q(\xi)) \end{array}\right] N_m(\xi)r(\xi)J(\xi)d\xi \quad (17)$$

$u_{r\,n}^{m}$ denotes the radial displacement component of n node in the m_{th} element. Each node on the boundary is taken in turn as the load point and the indicated numerical integration performed (ex. Gaussian quadrature) over the entire boundary, leading to a set of linear algebraic equations which can be finally given by

$$[H]\{u\}=[G]\{t\}+[V_1]\{\Phi\}+[V_2]\left\{\frac{d\Phi}{dn}\right\}$$
$$+\rho\omega^2\frac{(1-2\nu)}{2(1-\nu)}[W_1]+\rho\omega^2[W_2] \quad (18)$$

Matrices [H] and [G] contain the integrals of traction and displacement kernels, respectively, while $[V_1]$ and $[V_2]$ involve the integrals of thermoelastic kernels defined from Eq.(12), and $[W_1]$ and $[W_2]$ contain the integrals of the rotational body force kernels from Eq.(9). Before solving

Eq.(18), the boundary conditions are applied. These take the form of either prescribed displacement or tractions over each element. The equation can be rearranged such that all the unknown displacements and tractions are on the left hand side and all the known quantities including centrifugal and thermal loading terms are on the right and reduced the final stiffness equation as

$$[A]\{x\} = \{y\} \quad (19)$$

The stiffness [A] is in general fully populated with non-zero coefficients, and is not symmetric. The equation are best solved by direct elimination procedure like Gauss-Jordan technique.

Fig.2 shows the turbine rotor disk of an actual part of small turbojet engine structure(ADD 500) and for the present BEM analysis it is replaced by the three dimensional CAD configuration as shown in Fig.3. Due to symmetry only half the disk is modelled with 46 quadratic elements and 92 nodal points as shown in Fig.4.

The same disk is analyzed using the FEM with 104 quadrilateral elements and 135 nodal points as also shown in Fig.5. The material properties and loading data are as follows ;

Young's modulus, E	=	197.2 GPa
Poisson's ratio	=	0.3
mass density	=	8000 kg/m^3
rim loading	=	47.29 MPa
angular velocity, ω	=	4241.15 rad/s
Coefficient of thermal expansion	=	9.88×10^{-6}m/m ℃
temperature at inner surface, T_i	=	300 ℃
temperature at outer surface, T_o	=	900 ℃

The temperature distribution is prerequisite for such a boundary value problem. This can be obtained from an independent routine by solving the Laplace equation of steady-syate heat conduction.

Table 1. Comparison of BEM and FEM solution for the hoop stress in the turbine rotor disk

Radius $R\times 10$ (mm)	Temperature $\Phi\times 10^2$ (℃)	Temp. Gradient $d\Phi/dn\times 10$ (℃/ mm)	BEM Sol. $\sigma_\theta\times 10^2$ (MPa)	FEM Sol. $\sigma_\theta\times 10^2$ (MPa)
0.749	3.000	-1.676	9.584	-
0.940	3.292	0.0	7.936	8.550
1.295	3.711	0.0	5.764	6.371
1.422	4.037	0.0	4.751	4.992
2.007	3.213	0.0	4.206	4.399
2.362	4.562	0.0	3.882	4.109
2.692	4.784	0.0	3.696	3.896
3.073	5.040	0.0	3.509	3.647
3.581	5.390	0.0	3.254	3.482
4.013	5.699	0.0	2.965	3.185
4.394	5.976	0.0	2.641	2.675
4.750	6.232	0.0	2.468	2.324
5.080	6.465	0.0	2.144	1.931
5.385	6.671	0.0	1.779	1.627
5.690	6.862	0.0	1.393	1.317
6.020	7.052	0.0	1.041	0.965
6.350	7.236	0.0	0.896	0.820
6.655	7.416	0.0	0.800	0.958
6.934	7.601	0.0	0.669	0.869
7.163	7.771	0.0	0.469	0.607
8.052	8.545	0.0	-0.820	-0.586
8.306	8.760	0.0	-1.538	-1.558
8.463	8.876	0.0	-2.103	-2.310
8.651	9.000	0.632	-3.199	-

Fig.2 The turbine rotor disk of small turbojet engine

Fig.3 3-D Configuration of the turbine rotor disk

Fig.4 BEM meshes for the turbine rotor disk

Fig.5 FEM meshes for the turbine rotor disk

Table 1 shows the results of the BEM and FEM hoop stress solutions together with the corresponding temperature distribution, and Fig.6 depicts the comparison of these two stress distributions. Turbine disk is usually made thicker near its hub and taper down to a smaller thickness towards the periphery. The reason for this is the hoop stress concentration near center of rotation as clearly illustrated in Fig. 6. The BEM results of the radial stress distribution are also compared with the FEM one in Fig. 7. The close agreement between the BEM and FEM results confirms the accuracy of both model.

Fig.6 Hoop stress distributions in the turbine rotor disk

Fig.7 Radial stress distributions in the turbine rotor disk

4. CONCLUSIONS

The present study is an application of the BEM to the stress analysis problem for which axisymmetric body is subjected to thermal loading and highly rotational inertia body forces. An extension of the axisymmetric BEM formulation has been demonstrated to construct such kernel functions over equivalent boundary integrals. A discretization scheme is outlined for numerical treatment of the resulting boundary integral equations, and it is finally illustrated by solving the model problem of the turbine rotor disk for which a FEM solution has been furnished by author.

In order to achieve strength design for turbojet engine structure, further development of the BEM involves the capability to model transient thermal loading including thermal-dependent material properties.

REFERENCES

(1) Cruse, T. A., Snow, D. W. and Wilson, R. B., 1977, "Numerical Solutions in Axisymmetric Elasticity", Comp. & Struct., Vol.7, pp. 445 - 451.

(2) Bakr, A. A. and Fenner, R. T., 1983, "Boundary integral Equation Analysis of Axisymmetric Thermoelastic Problems", J. Strain Analysis, Vol. 18, pp. 239 - 251.

(3) Abdul-Mihsein, M. T., Bakr, A. A. and Parker, A. P., 1985, "Stresses in Axisymmetric Rotating Bodies Determined by the Boundary Integral Equation Method", J. Strain Analysis, Vol. 20, pp. 79 - 86.

(4) Rizzo, F. J. and Shippy, D. J., 1986, "A Boundary Element Method for Axisymmetric Elastic Bodies", Developments on BEM, Vol. 4(Banerjee and Watson Eds.) Elsevier Applied Sc. Pub., pp. 67 - 90.

(5) Kermanidis, T., 1975, "A Numerical Solutions for Axially Symmetrical Elasticity Problems", Int. J. Solids. Struct., Vol. 11, pp. 493 - 500.

(6) Bakr, A. A. and Fenner, R. T., 1983, "Use of the Hankel Transform in Boundary Integral Methods for Axisymmetric Problems", Int. J. Numer. Meths. Engng., Vol. 19, pp. 1765 - 1769.

(7) Hartmann, F., 1980, "Computing the C - Matrix in Non-smooth Boundary points", New Developments in BEM(Brrebia, C. A., Eds.) Butterworths, pp. 367 - 379.

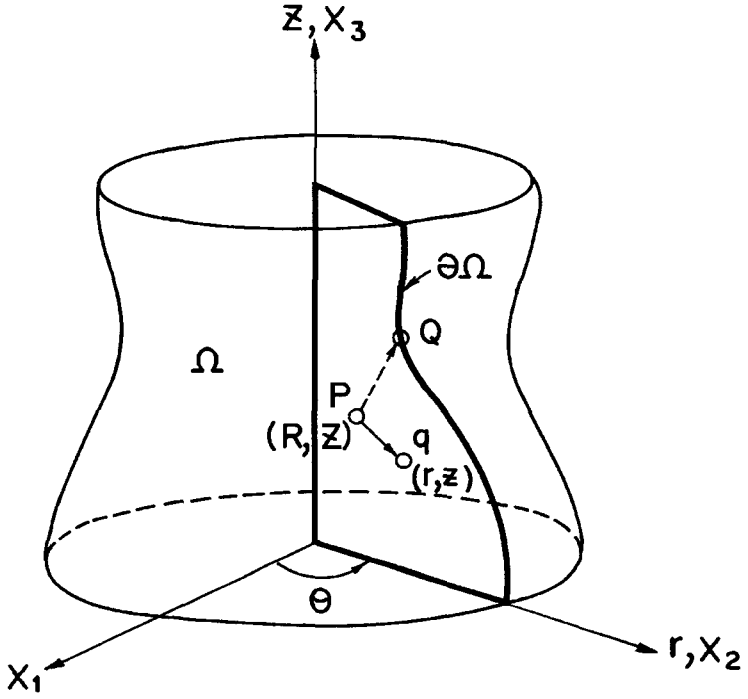

Fig.1 Geometry of the axisymmetric solution domain

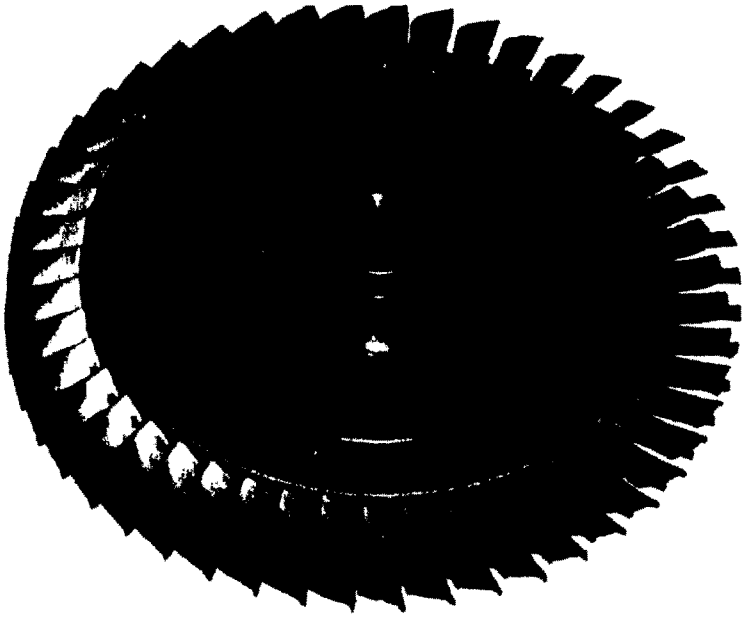

Fig.2 The turbine rotor disk of small turbojet engine

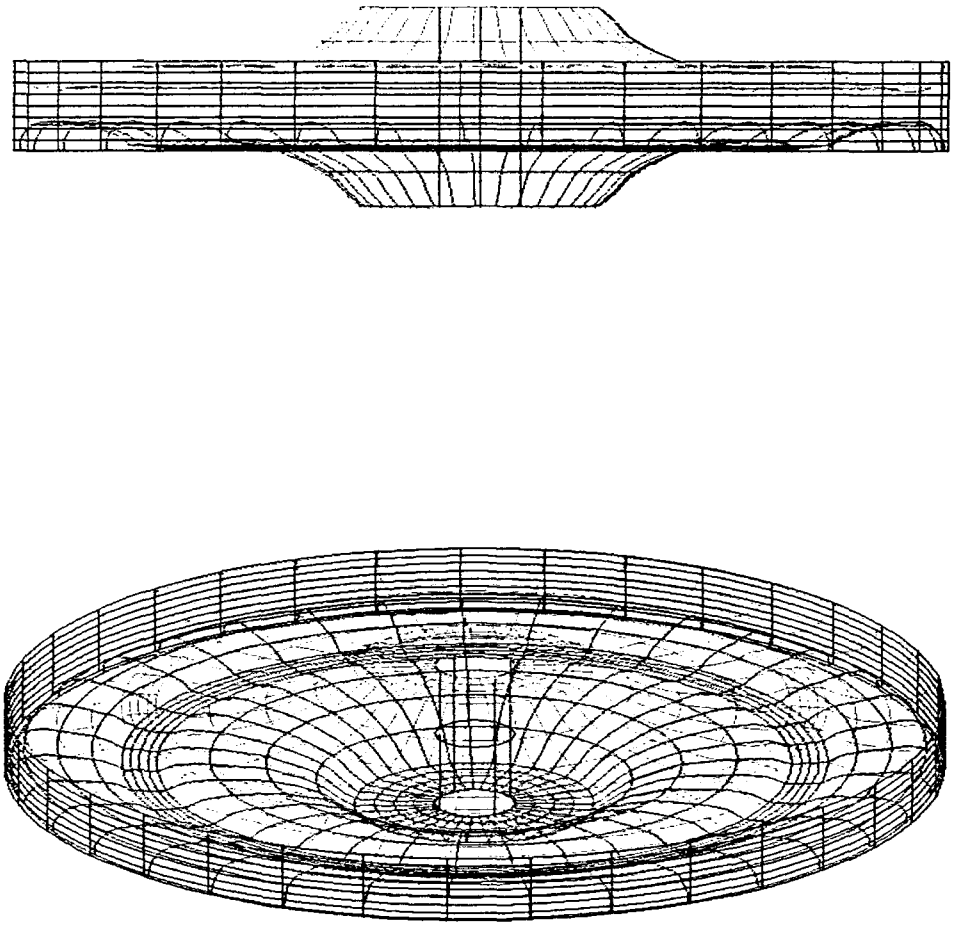

Fig3. 3-D Configuration of the turbine rotor disk

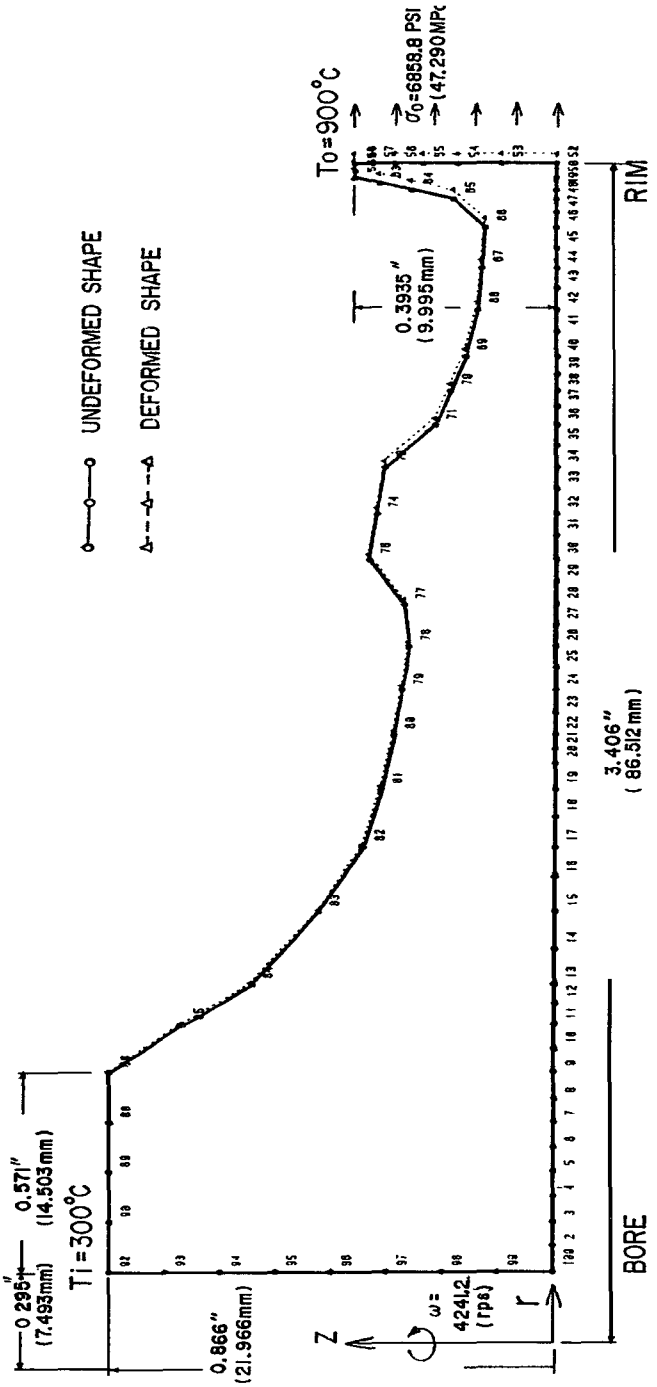

Fig4. BEM meshes for the turbine rotor disk

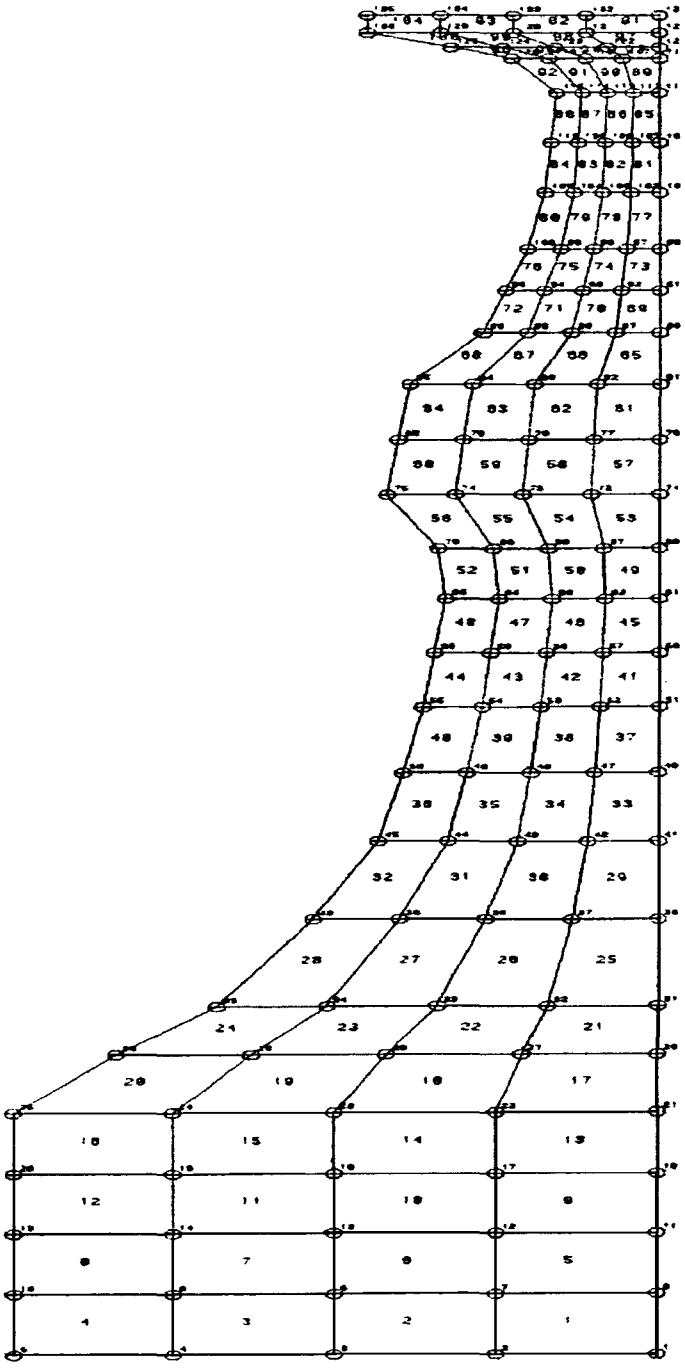

Fig.5 FEM meshes for the turbine rotor disk

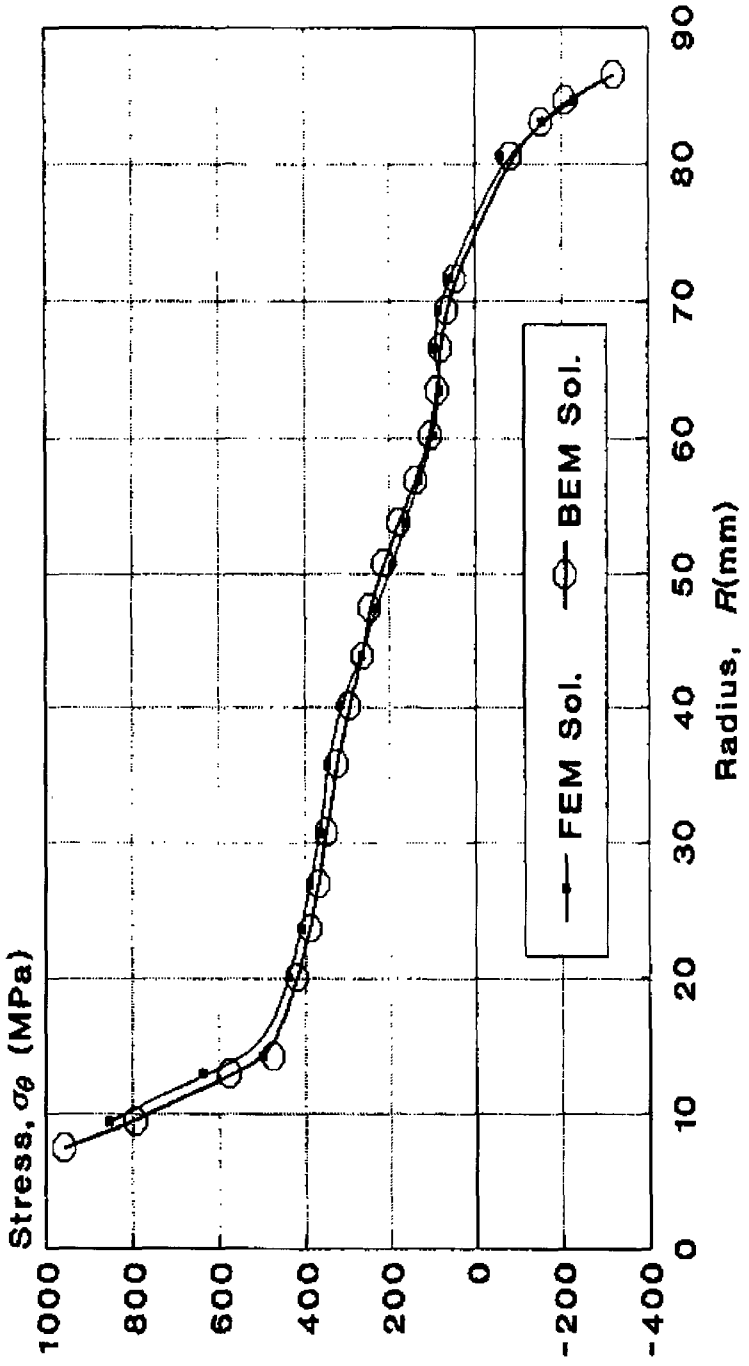

Fig.6 Hoop stress distributions in the turbine rotor disk

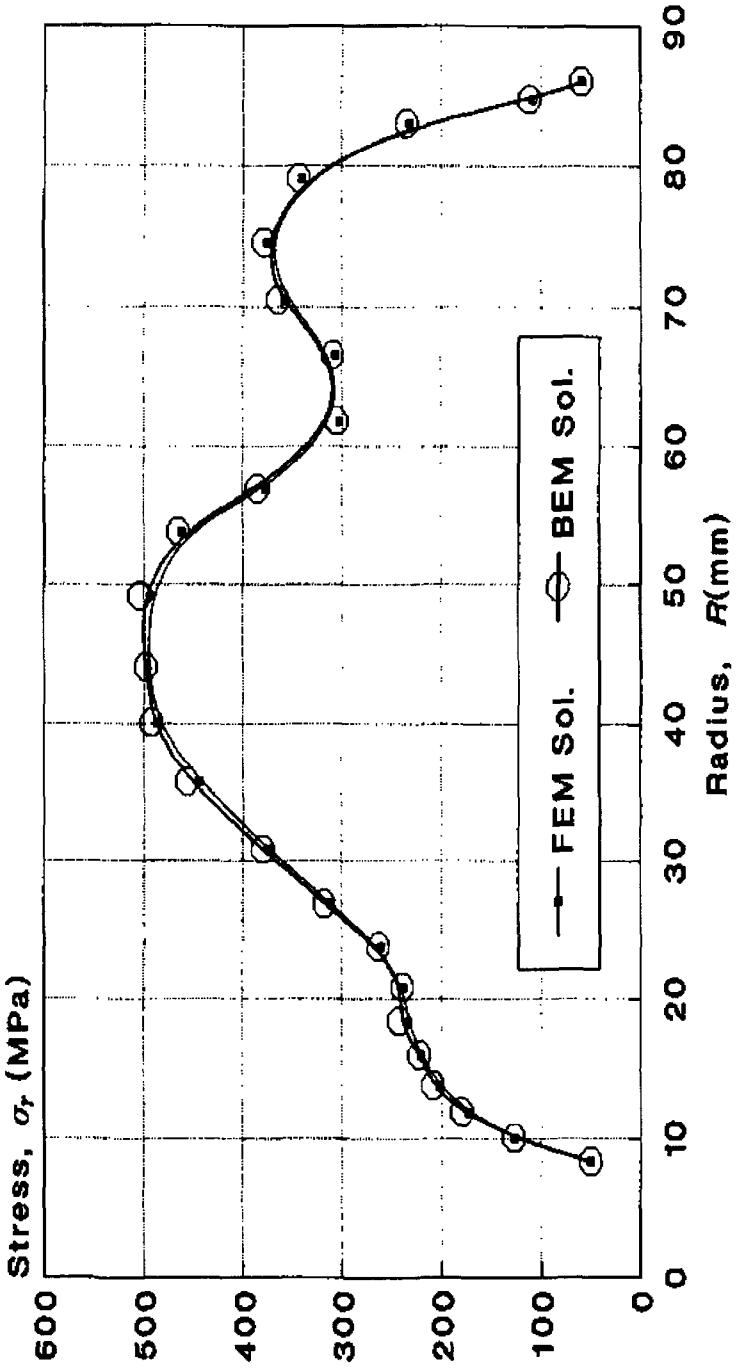

Fig.7 Radial stress distributions in the turbine rotor disk